AGU PUBLICATIONS

JGR

Journal of Geophysical Research: Biogeosciences

RESEARCH ARTICLE
10.1002/2017JG003958

Key Points:
- Isohydry/anisohydry estimates from backscatter and VOD data show reasonable agreement at low and middle latitudes but diverge at high latitudes
- Grasslands, croplands, and open shrublands are more anisohydric, while evergreen broadleaf and deciduous broadleaf forests are more isohydric
- VOD-based isohydry/anisohydry estimates show better agreement with upscaled in situ measurements than backscatter-based estimates

Supporting Information:
- Supporting Information S1

Correspondence to:
Y. Li and K. Guan,
yanli.geo@gmail.com;
kaiyug@illinois.edu

Citation:
Li, Y., Guan, K., Gentine, P., Konings, A. G., Meinzer, F. C., Kimball, J. S., … Good, S. P. (2017). Estimating global ecosystem isohydry/anisohydry using active and passive microwave satellite data. *Journal of Geophysical Research: Biogeosciences*, *122*, 3306–3321. https://doi.org/10.1002/2017JG003958

Received 22 MAY 2017
Accepted 18 OCT 2017
Accepted article online 13 NOV 2017
Published online 26 DEC 2017

©2017. American Geophysical Union. All Rights Reserved.

Estimating Global Ecosystem Isohydry/Anisohydry Using Active and Passive Microwave Satellite Data

Yan Li[1], Kaiyu Guan[1,2], Pierre Gentine[3,4], Alexandra G. Konings[5], Frederick C. Meinzer[6], John S. Kimball[7], Xiangtao Xu[8], William R. L. Anderegg[9], Nate G. McDowell[10], Jordi Martinez-Vilalta[11,12], David G. Long[13], and Stephen P. Good[14]

[1]Department of Natural Resources and Environmental Sciences, University of Illinois at Urbana-Champaign, Urbana, IL, USA, [2]National Center for Supercomputing Applications, University of Illinois at Urbana-Champaign, Urbana, IL, USA, [3]Department of Earth and Environmental Engineering, Columbia University, New York, NY, USA, [4]Earth Institute, Columbia University, New York, NY, USA, [5]Department of Earth System Science, Stanford University, Stanford, CA, USA, [6]Pacific Northwest Research Station, USDA Forest Service, Corvallis, OR, USA, [7]Numerical Terradynamic Simulation Group, College of Forestry and Conservation, University of Montana, Missoula, MT, USA, [8]Department of Geosciences, Princeton University, Princeton, NJ, USA, [9]Department of Biology, University of Utah, Salt Lake City, UT, USA, [10]Pacific Northwest National Laboratory, Richland, WA, USA, [11]CREAF, Cerdanyola del Vallès (Barcelona), Spain, [12]University Autònoma Barcelona, Cerdanyola del Vallès (Barcelona), Spain, [13]Department of Electrical and Computer Engineering, Brigham Young University, Provo, UT, USA, [14]Department of Biological and Ecological Engineering, Oregon State University, Corvallis, OR, USA

Abstract The concept of isohydry/anisohydry describes the degree to which plants regulate their water status, operating from isohydric with strict regulation to anisohydric with less regulation. Though some species level measures of isohydry/anisohydry exist at a few locations, ecosystem-scale information is still largely unavailable. In this study, we use diurnal observations from active (Ku-Band backscatter from QuikSCAT) and passive (X-band vegetation optical depth (VOD) from Advanced Microwave Scanning Radiometer on EOS Aqua) microwave satellite data to estimate global ecosystem isohydry/anisohydry. Here diurnal observations from both satellites approximate predawn and midday plant canopy water contents, which are used to estimate isohydry/anisohydry. The two independent estimates from radar backscatter and VOD show reasonable agreement at low and middle latitudes but diverge at high latitudes. Grasslands, croplands, wetlands, and open shrublands are more anisohydric, whereas evergreen broadleaf and deciduous broadleaf forests are more isohydric. The direct validation with upscaled in situ species isohydry/anisohydry estimates indicates that the VOD-based estimates have much better agreement than the backscatter-based estimates. The indirect validation with prior knowledge suggests that both estimates are generally consistent in that vegetation water status of anisohydric ecosystems more closely tracks environmental fluctuations of water availability and demand than their isohydric counterparts. However, uncertainties still exist in the isohydry/anisohydry estimate, primarily arising from the remote sensing data and, to a lesser extent, from the methodology. The comprehensive assessment in this study can help us better understand the robustness, limitation, and uncertainties of the satellite-derived isohydry/anisohydry estimates. The ecosystem isohydry/anisohydry has the potential to reveal new insights into spatiotemporal ecosystem response to droughts.

1. Introduction

Plants have evolved to develop a range of ecophysiological strategies to withstand drought (Akıncı & Lösel, 2012; Farooq et al., 2012; Matheny et al., 2016). Among others, stomatal closure is a central physiological strategy by which plants limit their transpirational water loss in order to avoid hydraulic failure at short timescales (Martínez-Vilalta & Garcia-Forner, 2016). The stringency of stomatal control differs among species and under various environmental conditions (Ball et al., 1987; Konings & Gentine, 2017; Martínez-Vilalta et al., 2014; Wong et al., 1979), and covaries with other plant hydraulic traits such as rooting depth (Martínez-Vilalta & Garcia-Forner, 2016; Matheny et al., 2016). The resulting varying levels of regulation of plant water status can be characterized by the concept of isohydry/anisohydry—the continuum from isohydric to anisohydric

behavior (Garcia-Forner et al., 2015; Landsberg & Waring, 2016; Martínez-Vilalta & Garcia-Forner, 2016; Martínez-Vilalta et al., 2014; McDowell et al., 2008; Meinzer et al., 2016; Tardieu & Simonneau, 1998). Broadly speaking, isohydric plants can maintain a relatively stable midday leaf water potential as environmental conditions (e.g., atmospheric water demand and soil water content) change, thereby dampening the diurnal and seasonal variations in leaf water potential (Martínez-Vilalta & Garcia-Forner, 2016; Meinzer et al., 2016). By contrast, anisohydric plants allow their leaf water potentials to closely track the fluctuations of environmental water availability and demand and thus exhibit greater diurnal and seasonal variations. The range of behavior from isohydric to anisohydric is closely linked to stomatal responses to water deficits (Sperry et al., 2016) and has important implications for understanding plant response to different drought conditions (Konings, Williams, et al., 2017; Roman et al., 2015).

Modeling water-vegetation interactions still presents a major challenge, particularly plants' responses to drought (McDowell et al., 2013). This is largely due to our knowledge gap in understanding these complex plant physiological behaviors at multiple scales (Fatichi et al., 2015; Landsberg & Waring, 2016). In current process-based terrestrial biosphere models, most representations of hydraulic processes are still simplistic and empirically based (Fatichi et al., 2015), limiting their ability to capture and predict plant responses to water stress as well as their feedbacks to climate (Xu et al., 2013). There has been increasing recognition of the need for incorporating plant hydraulic processes into mechanistic models to improve the representation of fundamental aspects such as plant water stress and recovery, drought sensitivity, and ultimately mortality (Anderegg et al., 2016; Bonan et al., 2014; Fatichi et al., 2015; Konings, Williams, et al., 2017; Xu et al., 2016). Understanding the role of isohydry/anisohydry, which is an integrated consequence of stomatal control, hydraulic traits, and their interactions with the environment, could provide new insights to help improve the modeling of key (physiological) processes related to plant water regulation.

Contemporary understanding of isohydry/anisohydry and attempts to quantify it primarily come from studies conducted at the plant or species levels (Klein, 2014; Martínez-Vilalta et al., 2014; Tardieu & Simonneau, 1998), whereas much less is known about the variation of isohydry/anisohydry at ecosystem to global scales. At the ecosystem scale, multiple species representing a range of isohydry to anisohydry coexist, but large-scale gradients (e.g., regional or global scales) in the overall ecosystem behavior may still occur. Ecosystem level isohydry/anisohydry information is more relevant to Earth system modeling (e.g., for model benchmarking and parameterization) than species level information, but it is not possible to obtain isohydry/anisohydry estimates at these large scales using traditional plant physiological methods. Spaceborne microwave remote sensing offers a unique opportunity. Both active and passive microwave remote sensing data are sensitive to vegetation water status, allowing them to be potentially useful for estimating ecosystem isohydry/anisohydry. Their sensitivities and ability to capture vegetation water status depend on operating frequency, overpass times, and physical properties of the land surface (Jones et al., 2011; Konings, Yu, et al., 2017; van Emmerik et al., 2015). Existing spaceborne records of both active and passive microwave have different characteristics on this front (Paget et al., 2016; Podest et al., 2014; Steele-Dunne et al., 2017). Recently, Konings and Gentine (2017) adapted the isohydry/anisohydry metric proposed by Martínez-Vilalta et al. (2014) to work with passive microwave satellite data from Advanced Microwave Scanning Radiometer on EOS Aqua (AMSR-E) and successfully produced the first global ecosystem-scale isohydry/anisohydry estimates. However, the reliability of such estimate from a single satellite record is uncertain due to potential sensor biases and retrieval errors. The degree to which these errors and varying sensitivities of microwave observation to vegetation water status affect the isohydry/anisohydry metric is unknown. Furthermore, a direct validation with in situ measurements is lacking.

This study improves upon recent work (Konings & Gentine, 2017) by addressing the aforementioned issues. First, we utilize both active and passive (with different retrieval algorithms) microwave satellite remote sensing data to provide new independent global isohydry/anisohydry estimates. Second, we validate these satellite-derived isohydry/anisohydry estimates through a cross comparison between them and a direct comparison with upscaled in situ species level estimates. Third, we perform an indirect validation by examining whether the observed response of plant water status to environmental fluctuations follows the expected theoretical pattern of isohydry/anisohydry. The overall aim of this study is to promote better understanding of satellite-derived ecosystem isohydry/anisohydry estimates and the robustness, limitations, and uncertainties of these estimates, their potential applications, and paths forward.

2. Data and Methods

2.1. Estimating Isohydry/Anisohydry From Microwave Satellite Data

Martínez-Vilalta et al. (2014) proposed a way to quantify the degree of plant isohydry/anisohydry using the slope of a linear regression fitted to the trajectory of the relationship between leaf and soil water potentials during a period of soil drying (equation (1)).

$$\Psi_L = \beta \cdot \Psi_S + \Lambda \tag{1}$$

Here Ψ_L and Ψ_S are leaf and soil water potentials, respectively. In practice, midday (Ψ_{midday}) and predawn ($\Psi_{predawn}$) leaf water potentials can be used as proxies of Ψ_L and Ψ_S by assuming plant and soil water potentials equilibrate ($\Psi_L \approx \Psi_S$) overnight when rehydration is complete. The slope β from equation (1) is an indicator for isohydry/anisohydry that usually varies from 0 to 1, though values less than 0 or greater than 1 occur occasionally. Zero represents strict isohydry and > 1 represents strict anisohydry. The intercept term Λ measures the (maximum) transpiration rate per unit of water transport capacity or, equivalently, the leaf water potential at $\Psi_S \approx 0$.

This method has been adapted by Konings and Gentine (2017) to work with remote sensing-based vegetation optical depth (VOD) data and to estimate isohydry/anisohydry at the ecosystem level during the growing season. The VOD retrieval from satellite passive microwave remote sensing defines the level of absorption and scattering of natural microwave emissions from the land surface by overlying vegetation. The VOD is sensitive to variations in vegetation biomass water content, while the effective range and penetration depth into vegetation depends on microwave wavelength (Jones et al., 2011). This adaptation of VOD for estimating isohydry/anisohydry is made possible by adopting a linear approximation of the relationship between leaf water potential and vegetation water content (proportional to VOD), which is a reasonable assumption and expected to incur only minimal relative error (see more details about this assumption in supporting information of Konings and Gentine (2017)). Note that vegetation water content here in the context of microwave remote sensing is defined as the mass of water per ground area which is different to the more physiological definitions (e.g., mass of water per mass of tissue or mass of water per unit of maximum water-holding capacity of the tissue). Therefore, equation (1) can be rewritten as equation (2) by replacing midday (Ψ_L) and predawn (Ψ_S) water potentials by midday VOD (1:30 p.m.) VOD_{midday} and midnight (1:30 a.m.) $VOD_{midnight}$, respectively.

$$VOD_{midday} = \beta \cdot VOD_{midnight} + \Lambda_{VOD} \tag{2}$$

Here we used the X-band (10.7 GHz) daily composite VOD data from Advanced Microwave Scanning Radiometer on EOS Aqua (AMSR-E) (Du et al., 2017) (http://ntsg.umt.edu/project/amsrelp#data-product), produced by the University of Montana (UMT) algorithm (Jones et al., 2011), for the period of 2002–2012, at a spatial resolution of 25 km. Compared to L-band VOD such as SMOS (Fernandez-Moran et al., 2017) or SMAP (Konings et al., 2016; Konings, Piles, et al., 2017), the X-band VOD from higher frequency is relatively more sensitive to leaves rather than stems and is more suitable for representing vegetation water status. Alternative algorithms exist for retrieving VOD such as the Land Parameter Retrieval Model (LPRM) (Meesters et al., 2005; Owe et al., 2008), which was the data set used in Konings and Gentine (2017). One major difference between the UMT and LPRM algorithms is the treatment of open surface water, which can influence the VOD retrievals. Isohydry/anisohydry estimates based on the two VOD data sets with different algorithms are compared and discussed in the section 3. To simplify terminology, if not specified, either "AMSR-E VOD" or "VOD-based estimate" throughout the paper refers to the isohydry/anisohydry estimated using the UMT VOD data. While the estimate from LPRM VOD data (the same data set used by Konings & Gentine, 2017) is referred to as "LPRM VOD" for comparison purpose which appears in Figure 2.

The backscatter coefficient (referred to here as σ^0) from satellite radar scatterometry is another independent and remotely sensed measurement. Similar to VOD, σ^0 exhibits wavelength-dependent sensitivity. While longer wavelength backscatter measurements carry more information about the whole canopy due to stronger radar penetration ability (Konings, Yu, et al., 2017), short wavelength backscatter retrievals tend to be more sensitive to vegetation water content variations of the upper canopy layer (Kim et al., 2012; Konings, Yu, et al., 2017; van Emmerik et al., 2015; van Emmerik, Steele-Dunne, Judge, et al., 2017) and associated derivatives, including vegetation biomass (Frolking et al., 2005; Guan et al., 2012), water stress (Steele-Dunne et al., 2012; van Emmerik et al., 2015; van Emmerik, Steele-Dunne, Paget, et al., 2017), and phenology (Frolking et al., 2006; Guan et al., 2014). Unlike VOD, the radar backscatter coefficient is more sensitive to vegetation

canopy orientation, structure, and incidence angle, which we assume exhibit negligible diurnal variations between morning and afternoon overpasses at the scale of the satellite retrieval due to its coarse spatial resolution. By assuming a linear relationship between σ^0 and vegetation water content (Kim et al., 2012; van Emmerik et al., 2015), equation (2) can be rewritten as equation (3) to work with backscatter data. Note that σ^0 and vegetation water content has a relationship close to linear over the range of backscatter, but the σ^0 response can exhibit saturation at high vegetation water content, as shown in van Emmerik et al. (2015). This could lead to some errors but expected to be relatively small.

$$\sigma^0_{\text{afternoon}} = \beta \cdot \sigma^0_{\text{morning}} + \Lambda_{\sigma^0} \tag{3}$$

Here we used global (daily or 4 day composite depending on region) Ku-band (13.4 GHz) satellite radar backscatter data from QuikSCAT, extending from 1999 to 2009 and including both V and H polarizations processed, at an enhanced spatial resolution of 5 km (available at http://www.scp.byu.edu) (Long & Hicks, 2010). The Ku-Band radar backscatter signal is more suitable than longer microwave wavelength data for many vegetation applications because of its greater sensitivity to the upper canopy layer (Waring et al., 1995). The QuikSCAT morning (6 a.m., ascending mode) and afternoon overpass (6 p.m. descending mode) data are used as a proxy for respective predawn and midday conditions, though the 6 p.m. sampling is not ideal because midday water potentials may be more negative than observed later in the day, causing potential isohydry/anisohydry underestimation (i.e., isohydric bias). Similarly, the midnight overpass time of AMSR-E VOD at 1:30 a.m., which is used to represent predawn condition, can lead to potential isohydry/anisohydry overestimation (i.e., anisohydric bias) due to the incomplete equilibration at midnight relative to predawn conditions. The influence of overpass time was further investigated by comparing the isohydry/anisohydry estimates between QuikSCAT and another satellite backscatter from OSCAT (2009–2013, http://www.scp.byu.edu/data/OSCAT/SIR/OSCAT_sir.html), which has the same Ku-Band operating frequency as QuikSCAT but a different overpass time of 12:00 a.m./p.m. instead of 6 a.m./p.m. (see section 4).

Before estimating isohydry/anisohydry, σ^0 and VOD data on rainy days (i.e., days with nonzero precipitation) were filtered using daily Global Precipitation Climatology Project precipitation (1°) data (ftp://meso.gsfc.nasa.gov/pub/1dd-v1.2/). This filtering helps avoid the influence of rainfall intercepted water in the canopy layers on canopy water content and the atmospheric impact on the σ^0/VOD measurements. Due to the frequent gaps in the daily data and its regionally uneven availability, we averaged all available values with outliers removed to obtain half-monthly values for both σ^0 and VOD. In addition, we used a long-term climatology of 16 day Moderate Resolution Imaging Spectroradiometer (MODIS) Enhanced Vegetation Index (EVI) data at 0.05° (MOD13C1) to define a vegetated season for each grid cell, calculated as the period when EVI is greater than 0.3 (Figure S1 in the supporting information). This threshold was chosen to balance spatial coverage and allowing for a sufficiently high remaining number of samples. Constraining our analysis within this vegetated season ensures that the land surface is covered by vegetation with minimal bare soil influence expected on σ^0. In regions where soil freezes during part of the year, this threshold also corresponds to the nonfrozen season so that the effects of freezing and seasonal snow cover on the microwave observations are diminished. The resulting diurnal half-monthly time series of σ^0 and VOD during the vegetated season are used to estimate isohydry/anisohydry for each pixel at the native spatial resolutions, following equations (3) and (2). When needed, the median resampling method was used to upscale the results from their native spatial resolution to coarser resolution. In this paper we mainly focus on the slope of the regression (i.e., β, the isohydry/anisohydry indicator), while the intercept term Λ (which is given by the regression outputs) is not discussed. This is because the original physical meaning of Λ based on water potential may no longer hold when microwave satellite observations are used instead (i.e., the Λ in equations (2) and (3)), and Λ is shown to be highly correlated with the estimated slope (Martínez-Vilalta et al., 2014). Since the two polarizations (H and V) of QuikSCAT show similar results though their sensitivities to vegetation could differ (van Emmerik et al., 2015), we only report V-polarization σ^0 results in the main text while the H-polarization results are provided in the supporting information.

2.2. Direct Validation With Upscaled In Situ Estimates

The work of Martínez-Vilalta et al. (2014) included isohydry/anisohydry estimates for 102 species using equation (1). Species were classified into four plant functional types (PFTs) based on their growth form and phylogeny: conifer, broadleaf, shrub, and herb, using information reported in the literature. Here we used plant species occurrence information from the Global Biodiversity Information Facility (GBIF) and grid area fraction

from MODIS land cover data to upscale the in situ measurements (see workflow in Figure S2). The Global Biodiversity Information Facility is an international open data infrastructure that provides data access to evidence about more than 1.6 million species around the world, collected over three centuries of natural history exploration and including current observations from citizen scientists, researchers, and automated monitoring programmes. The upscaling enables a more direct comparison between satellite-based and in situ isohydry/anisohydry estimates. First, we extracted occurrence records for each species after the year 1990 from the large GBIF database (http://www.gbif.org/occurrence/search?TAXON_KEY=6, retrieved on 17/01/2017) and aggregated the occurrence of each species (total number) to a 1° grid cell based on geolocation information. Second, the 13 IGBP MODIS land cover types were combined into 7 PFT groups at 1° spatial resolution to obtain their areal fraction (Table S1). The seven PFT types are composed of either conifer, broadleaf, shrub, and herb or their combinations. The estimate value at each grid cell can be derived based on the grid level species occurrence frequency and fractional area of each PFT group from steps 1 and 2. We first calculated the species-frequency-weighted mean estimate value for each PFT group on a per-grid cell basis, and the PFT-area-weighted mean estimate value (by the fractional area of each PFT group) gives the final grid cell level estimates.

2.3. Indirect Validation With Vegetation Water Response to Environmental Fluctuations

An indirect method of validation is to check whether the observed vegetation water response to environmental fluctuations is consistent with what is expected from its estimated isohydry/anisohydry. The underlying theory is that isohydric species maintain relatively stable midday water potential as environmental conditions change (largely as a result of their strict stomata control), whereas midday water potential in anisohydric species more closely tracks environmental fluctuations (e.g., atmospheric water demand and soil water content) (Martínez-Vilalta et al., 2014). Therefore, one would expect that a greater fraction of the variation of daytime σ^0/VOD signals (which are representative of midday water potential) could be explained by the environmental fluctuation of water availability and demand in anisohydric ecosystems than in isohydric ecosystems.

To test above hypothesis, we used air temperature, vapor pressure deficit, and precipitation from the Climate Research Unit and shortwave radiation from the Clouds and the Earth's Radiant Energy System for the same period as the satellite σ^0/VOD records to represent environmental conditions of water availability and demand. Since these variables are highly correlated with each other, we performed a principal component analysis (PCA) and extracted the first two leading components. These two components can explain more than 90% of total variance in most parts of the world and ~ 80% in tropical regions (Figure S3). We then calculated the R^2 between monthly time series of daytime σ^0 (and VOD) and the two leading PCA terms, which represent how much variation of σ^0 (and VOD) can be explained by environmental conditions.

3. Results

Figure 1 shows ecosystem isohydry/anisohydry estimated from QuikSCAT σ^0 and AMSR-E VOD at the global scale. The two data sets exhibit overall similarity with each other and also contain noticeable spatial mismatch. Estimated isohydry/anisohydry for most ecosystems lies in the range between extremely isohydric (β=0) and anisohydric (β >1), but some negative values occur, especially for the σ^0-based estimate. Highly isohydric ecosystems can be found in wet tropical regions (Amazon, Africa, and Asia), indicated by a very low β value from both data sets. These regions generally correspond to tropical forests (particularly for σ^0-based estimate) which are known to be isohydric (Fisher et al., 2006; Konings & Gentine, 2017), and both microwave satellite sensors mostly observe upper canopy information overlying this dense, multilayer vegetation. Other ecosystems that show relatively isohydric behaviors in both data sets are located in the southeast U.S., west and central Europe, and the majority of Eurasia. Highly anisohydric ecosystems can be seen in northern India and the North China Plain where arid land and croplands are abundant and also in Scandinavia with widespread alpine coniferous forest cover. Despite the global similarity, σ^0- and VOD-based isohydry/anisohydry estimates also show some differences at local and regional scales. For example, for some areas in South America and southern Africa, the high β observed in the VOD-based estimate is not seen in the σ^0 results. In the northern high latitudes (i.e., north of 45°N) of Siberia, β estimated from VOD is generally lower than the σ^0 results. In Scandinavia, the sharp contrast between northern (isohydric) and southern (anisohydric) parts of the peninsula in the σ^0 results does not appear in the VOD-based estimation.

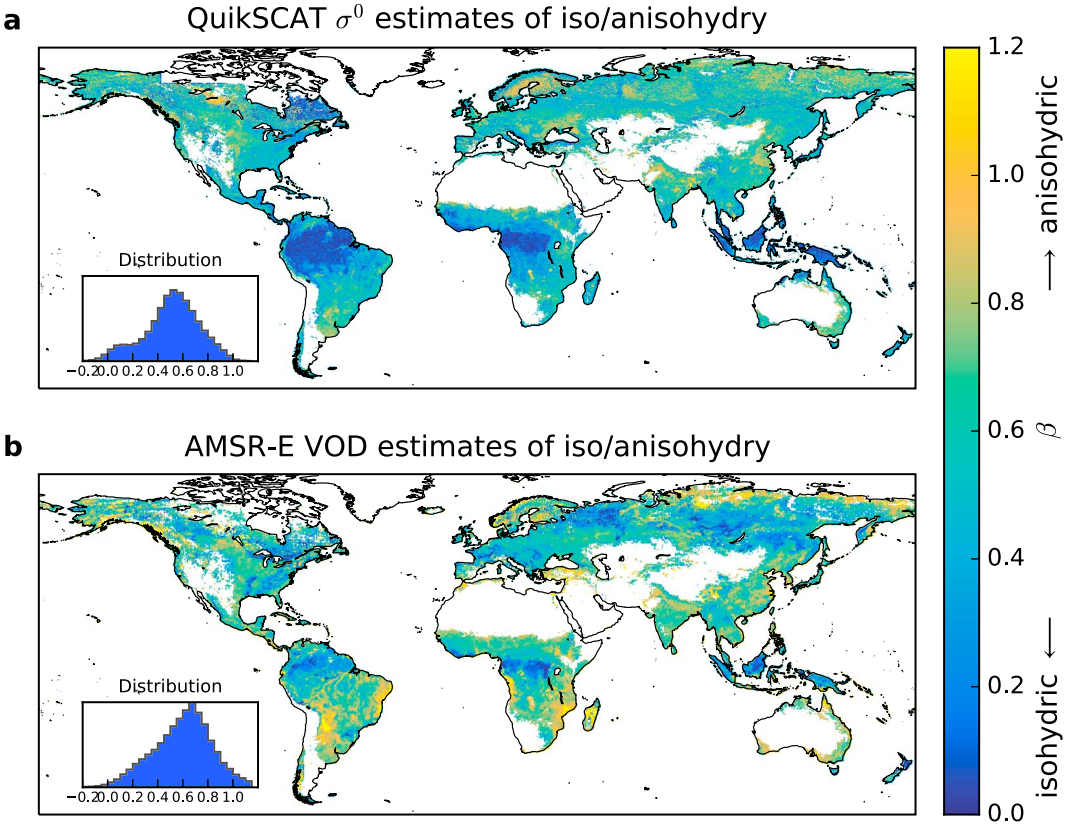

Figure 1. Global isohydry/anisohydry estimates from (a) QuikSCAT V-polarization σ^0 (0.05°) and (b) AMSR-E VOD (UMT, 0.25°). Insets show the distribution of the estimates. The indicator of isohydry/anisohydry is the slope (β) of the regression in equation (1) or equation (2). Slope values near 0 indicate extreme isohydric behavior, and values >1 indicate extreme anisohydric behavior. The differences between the two estimates and their confidence interval range are provided in Figure S5, and a similar figure for QuikSCAT H-polarization σ^0-based estimate is provided as Figure S4.

To evaluate the spatial consistency of the different isohydry/anisohydry estimates quantitatively, we computed the spatial correlation between each pair of estimates from four data sets including QuikSCAT V- and H-polarization σ^0, AMSR-E VOD of this study (UMT VOD), and LPRM VOD reprocessed with the method of this study. At the global scale (Figure 2a), the two σ^0-based estimations from H and V polarizations have the highest correlation with each other ($r = 0.92$), while both estimates have much lower correlations with the UMT VOD-based estimates in this study (r: 0.30 – 0.34) and slightly higher correlation with the LPRM VOD-based estimation (r: 0.47 – 0.49).

The isohydry/anisohydry estimates from the different data sets agree relatively well with each other in low- and middle-latitude areas but diverge at higher latitudes. The spatial correlations calculated in middle and low latitudes are much higher ($r > 0.50$; Figure 2c) compared to those in the northern high latitudes ($r < 0.27$ excluding QuikSCAT σ^0; Figure 2b). The low agreement of isohydry/anisohydry estimates in the northern high latitudes (north of 45°N) can be traced back to the higher uncertainties in the slope estimation β in this region, as indicated by the relatively greater range of the confidence interval (95% t test) for both σ^0- and VOD-based estimates (Figure S5). In particular, the LPRM VOD-based estimation, despite its good agreement in low and middle latitudes, shows a quite different pattern in high latitudes, with an overall higher slope β (Figure S6), resulting in very low correlations (Figure 2b) not only with σ^0- ($r < 0.10$) but also with the UMT VOD-based estimation ($r = 0.19$). This discrepancy between the two VOD-based estimates at high latitudes is likely caused by the differences of the VOD retrieval algorithms over wetter areas. Compared to the UMT algorithm, the LPRM algorithm does not account for the influence of open water variability on the VOD retrieval, and open water is commonly seen at the northern high latitudes (Pekel et al., 2016). It is worth noting that though the UMT algorithm accounts for the surface open water fraction in the VOD retrieval (Jones et al., 2011, 2016), the VOD results may still be affected by the residual contamination. The σ^0 signals are also sensitive to open water

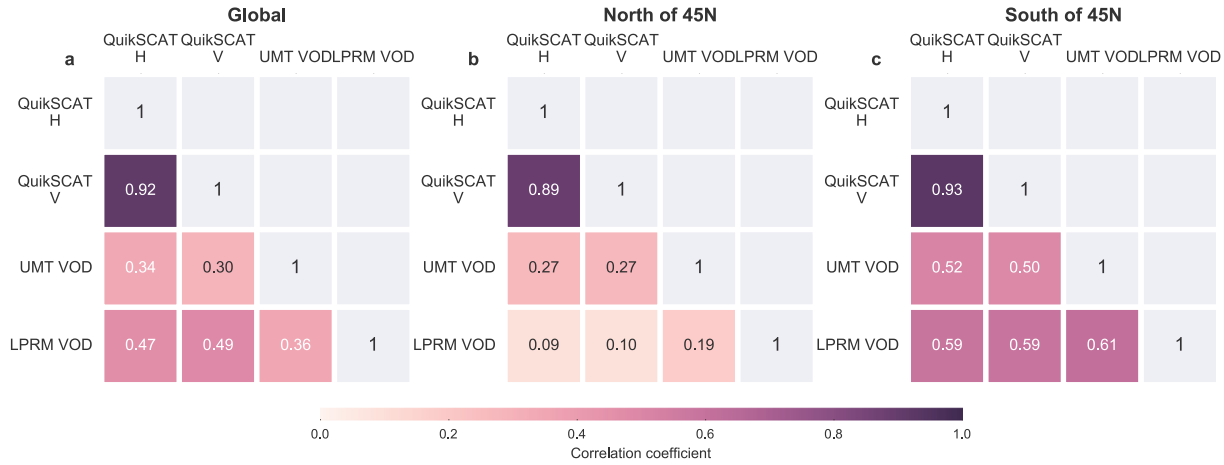

Figure 2. Spatial correlations of isohydry/anisohydry estimates between different data sets in (a) global, (b) north of 45°N, and (c) south of 45°N. Four data sets included are QuikSCAT H- and V-polarizatoin σ^0 and AMSR-E VOD from two sources: UMT VOD and LPRM VOD. The LPRM VOD isohydry/anisohydry map is provided in Figure S6. The Pearson correlation between data set is calculated at 1° resolution. The region north of 45°N is referred to as northern high latitude. It also corresponds to the area where isohydry/anisohydry estimates between QuikSCAT and AMSR-E have larger differences.

(Kimball et al., 2004), as water lowers the σ^0 value. However, correcting the effect of open water bodies on σ^0 is not straightforward, as the effect is also dependent on surface roughness which is affected by local winds (Ulaby & Long, 2014). The QuikSCAT σ^0 data were produced from higher spatial resolution images which can help to alleviate contamination from small water bodies, because permanent surface water has been filtered by applying the EVI threshold at the native resolution of the data.

Figure 3 compares QuikSCAT V-polarization σ^0-based and AMSR-E VOD-based (from the UMT algorithm) isohydry/anisohydry estimates for the major MODIS IGBP land cover types. Note that only 12 out of 13 land cover types are shown in Figure 3 because there were too few samples for closed shrublands at the 1° resolution considered here. Positive correlations are observed for all land cover types except for permanent wetlands, where both active and passive microwave data are affected by the presence of surface water bodies. Despite regional differences shown in Figure 1, the general positive correlation between the two types of data again confirms the broad consistency between σ^0- and VOD-based estimates. Nevertheless, the estimated isohydry/anisohydry has noticeable variations among different land cover types. The isohydry/anisohydry indicator β varies from the lowest mean value (0.21) in evergreen broadleaf forests (σ^0) to the highest mean value (0.75) in Savannas (VOD). Among the 12 land cover types, grassland, cropland, wetland, and open shrublands consistently have the highest β in both σ^0- and VOD-based estimates (Figures 3 and S8). However, land cover types with the lowest β are not consistent between the two estimates. For certain land cover types, the difference between two estimates can be larger than 0.20 (e.g., evergreen broadleaf forests, deciduous broadleaf forests, and savanna). Nevertheless, evergreen broadleaf forests and deciduous broadleaf forests show the lowest β in at least one of the two estimates. It should be noted that the estimates of β vary significantly within a specific land cover type, as also discussed in Konings and Gentine (2017). In fact, the differences observed between land cover types reflect not only the different vegetation characteristics pertaining to each land type but also the regional differences (e.g., in climate and species) embedded in the nonuniform geographic distribution of each land cover class.

Comparisons of the upscaled GBIF in situ isohydry/anisohydry measure with the QuikSCAT σ^0- and AMSR-E VOD-based estimates are shown in Figure 4. The GBIF estimate mainly covers the U.S. and Europe but with fewer estimates in other parts of the world. The limited coverage is primarily constrained by the geographical distribution of selected species. At each grid cell, the total number of occurrence records and the areal fraction of PFT groups with isohydry/anisohydry values vary greatly (Figure S9). Both factors affect the representativeness of grid cell level estimates and thus should be taken into account in the comparison. For this reason, here we only used grid cells with a relatively large number of records (>1,000) and with full PFT sampled (i.e., all PFT groups in the grid cell have isohydry/anisohydry values) for the comparison with the σ^0-based (Figure 4b) and VOD-based estimates (Figure 4c).

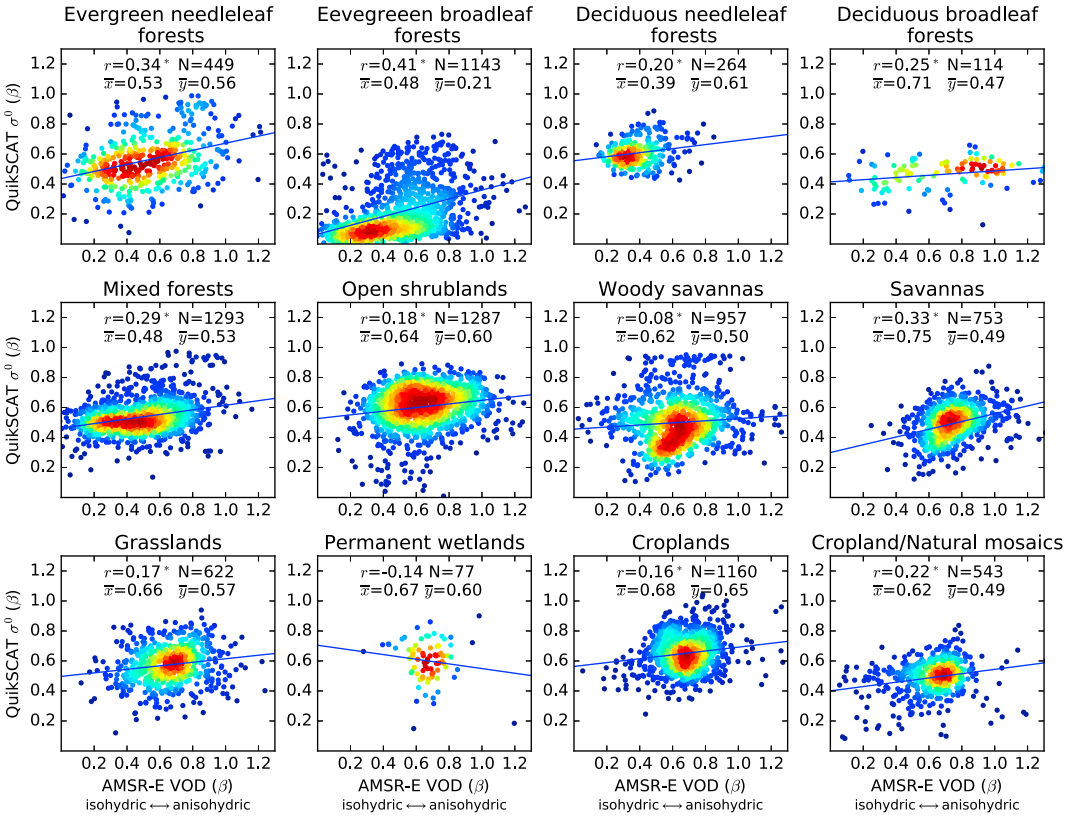

Figure 3. Isohydry/anisohydry estimates between QuikSCAT V-polorization σ^0 and AMSR-E VOD for 12 IGBP land cover types. In each panel, *r* is the Pearson correlation (asterisk denotes significance at 95%), *N* is the number of data points, and $\bar{x}$ and $\bar{y}$ are averages of VOD- and σ^0-based estimates, all at 1°. Color shows the relative density of data points estimated using Gaussian kernels, with higher density in red and lower density in blue. Similar figure for QuikSCAT H-polarization σ^0-based estimate is provided as Figure S7.

Over the selected GBIF grid cells (mainly Western Europe), the σ^0-based estimates have a negative relationship with GBIF ($r = -0.25$ for QuikSCAT V-σ^0 and $r = -0.31$ for H-σ^0), while the VOD-based estimates have a positive relationship ($r = 0.43$ for AMSR-E VOD in Figure 4 but a weaker $r = 0.12$ for LPRM VOD in Figure S10). Both the negative and positive correlations become larger in magnitude and reach higher significance levels when more strict criteria are applied to the grid cell selection (i.e., higher threshold for the number of occurrence records of each grid cell, Figure S11). The negative correlation between σ^0-based and GBIF estimates is unexpected, probably due to the σ^0 signal in Western Europe not being able to capture vegetation variability as well as VOD (see Figure 7 in section 4). Nevertheless, this result suggests that at least over the limited GBIF grid cells in Western Europe, the VOD-based estimate is more consistent with upscaled in situ estimates while the σ^0-based estimate is not. This can be further confirmed when breaking the comparison into PFT groups. At the individual PFT level, we observed positive correlations between VOD-based and GBIF estimates in five out of seven PFT groups consisting of trees (conifer and broadleaf) and herb (Figure S12), but there was only one PFT group (broadleaf) in the σ^0 results that had a positive correlation with GBIF (Figures S13 and S14). In general, the isohydry/anisohydry estimate from VOD agrees better with GBIF in situ estimates than that from σ^0. However, the results of this comparison should be interpreted with caution, because the 102 species used to produce the isohydry/anisohydry upscaled map may be insufficient to fully represent ecosystem-scale information at the coarse grid scale (1°), and their occurrence in the GBIF database could be biased, with limited spatial coverage.

The indirect validation results provide positive evidence to support a reasonable estimate of isohydry/anisohydry from QuikSCAT σ^0 and AMSR-E VOD. The σ^0 results (Figure 5a) show that the variability of daytime vegetation water content (represented by afternoon σ^0) explained by environmental fluctuations (R^2) increases along the estimated continuum from isohydry to anisohydry. The VOD results also show an increasingly larger variability in daytime vegetation water content (represented by midday VOD) explained by environmental

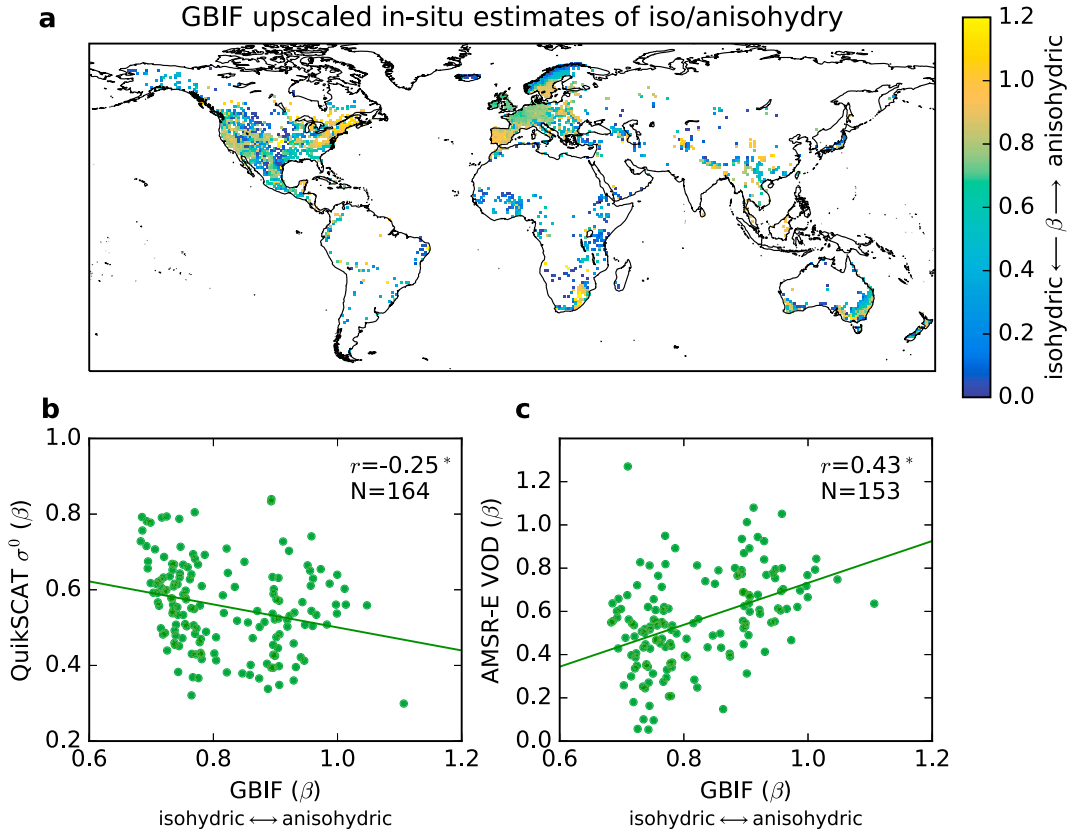

Figure 4. Comparison of satellite isohydry/anisohydry estimates (β) with upscaled in situ measures. (a) In situ isohydry/anisohydry measurements of 102 species from (Martínez-Vilalta et al., 2014) are upscaled to 1° resolution based on species occurrence records from the GBIF database and MODIS land cover data (see supporting information; hereafter GBIF estimate). (b) Scatterplot between GBIF and QuikSCAT V-polarization σ^0-based estimates. (c) Scatterplot between GBIF and AMSR-E VOD-based estimates (from the UMT algorithm). In Figures 4b and 4c, only data points of GBIF estimates with species occurrence records >1,000 and full PFT sampled are shown to ensure their representativeness at the ecosystem level. *r* is the Pearson correlation (asterisk denote significant at 95%), and *N* is the number of data points.

fluctuations toward anisohydry (when $\beta > 0.35$) (Figure 5b). These validation results are generally consistent with our prior knowledge that vegetation water content of anisohydric plants tracks environmental fluctuations more closely than isohydric counterparts. However, the specific patterns of σ^0 and VOD are not the same and neither of them show a monotonic increase over the full isohydry/anisohydry range but with some bumps and dips at certain β ranges. For example, the variance explained by PCA1+2 can decrease along the isohydry/anisohydry gradient when β is below 0.35 for VOD and when β is between 0.55 and 0.75 or greater than 0.95 for the σ^0-based estimate. The drop in R^2 can also be found in the indirect validation results broken into land cover types (Figures 5c and 5d). It seems that the drop in R^2 with the increasing β in the σ^0-based estimate ($0.55 < \beta < 0.75$) is more land cover-type dependent, while the drop in VOD-based estimate ($\beta < 0.35$) is uniform across all land cover types. These results indicate that despite the overall positive relationship, there are noticeable regional differences between σ^0- and VOD-based estimates, which means that the same β range may not always correspond to the same region. For example, the spatial range of $\beta < 0.35$ given by VOD includes a much smaller area in the Amazon than the σ^0-based estimate and a large area in the northern high latitude where σ^0-based estimate gives much higher β.

4. Discussion

The degree of isohydry/anisohydry estimated from microwave satellite data demonstrates a feasible new way of estimating ecosystem level information about the stringency of regulation of plant water status, which is difficult to obtain with traditional methods. The estimated isohydry/anisohydry here should not be interpreted as a constant but rather as a mean state over a relatively long time period (10 years in this study), as seasonal variations like phenology may have been included in the estimation. In reality, plant isohydry/

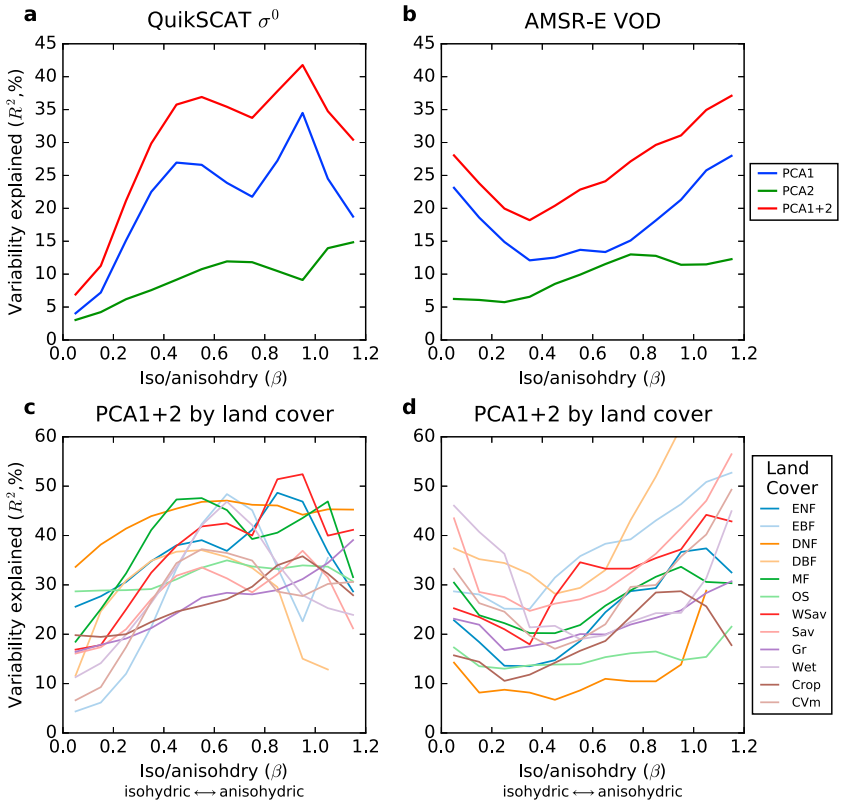

Figure 5. Temporal variability of daytime (a) QuikSCAT V-polarization σ^0 and (b) AMSR-E VOD explained by environmental fluctuations (R^2) along their estimated isohydry/anisohydry gradient (β). Environmental condition is represented by the first (PCA1) and second (PCA2) leading principal components of the PCA performed on monthly mean temperature, vapor pressure deficit, precipitation, and surface shortwave radiation. R^2 indicates how much variability of σ^0 or VOD can be explained by the PCA (%). Each data point represents the average R^2 for the corresponding isohydry/anisohydry bin at a width of 0.1. (c, d) PCA1+2 decomposed of 12 IGBP land cover types. Land cover type abbreviations: 1, evergreen needleleaf forest (ENF); 2, evergreen broadleaf forest (EBF); 3, deciduous needleleaf forest (DNF); 4, deciduous broadleaf forest (DBF); 5, mixed forest (MF); 7, open shrublands (OS); 8, woody savannas (WSav); 9, Savannas (Sav); 10, grasslands(Gr); 11, Permanent wetlands (Wet); 12, croplands (Crop); 14, cropland/natural vegetation mosaic (CVm).

anisohydry behavior is much more complicated than that represented by the metric β (equation (1)). It is known that some plants can even switch between isohydric and anisohydric behaviors based on environmental conditions (Domec & Johnson, 2012; Schultz, 2003) and can exhibit seasonal changes (Konings & Gentine, 2017). These dynamics could potentially be captured by our methodology utilizing continuous observations of microwave satellite data over a long time span combined from various microwave sensors such as QuikSCAT, ASCAT, RapidSCAT, AMSR-E, and AMSR-2.

Despite these encouraging findings, remotely sensed isohydry/anisohydry contains a number of important uncertainties resulting from both methodology and satellite data that can serve as avenues for future research. First, the methodology for estimating isohydry/anisohydry employed here is based on several assumptions introduced by Martínez-Vilalta et al. (2014) in their water potential framework and by Konings and Gentine (2017) in the adaptation of satellite data. These important assumptions include (A1) the steady state condition at daily to seasonal timescales (i.e., water transport through the xylem is balanced with leaf transpiration losses, without considering capacitance), (A2) a linear relationship between midday and predawn plant water potentials, (A3) soil and plant water potentials that are in equilibrium in the predawn or nighttime satellite overpass time, and (A4) a linear relationship between the water status measurement (σ^0 or VOD) and water potential. In most cases, these are reasonable assumptions. As discussed in Martínez-Vilalta et al. (2014): A1 is a reasonable first approximation and is consistent with previous studies. The linear function in A2 has been tested and reveals that the linear relationship can give a better fit and greater explained variance compared to nonlinear functions (Martínez-Vilalta et al., 2014). A3 and A4 can cause some errors to the estimate of β as

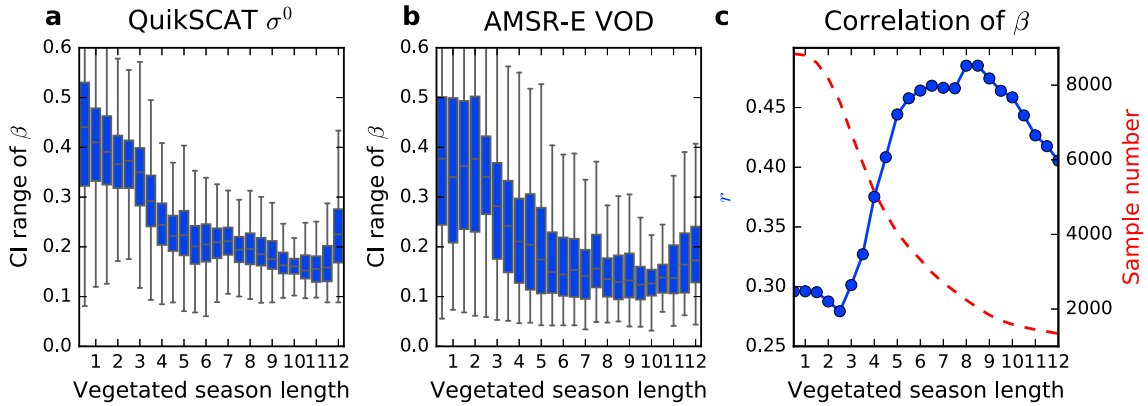

Figure 6. The uncertainty range of the (a) QuikSCAT σ^0-based, (b) AMSR-E VOD-based isohydry/anisohydry estimates, and (c) their correlations as a function of vegetated season length. The uncertainty range in Figures 6a and 6b is represented by the confidence interval (CI) range of β in the regression estimates at 95% significance level. The boxplot shows the CI range of isohydry/anisohydry estimates across different vegetated season lengths (unit in month). Figure 6c shows the spatial correlation (r in blue) between σ^0-based and VOD-based isohydry/anisohydry estimates across vegetated season length. Correlation is calculated using a subset of grids that have the vegetated season longer than the threshold shown on the x axis at 1°, and the dashed line (red) shows the sample number of grid cells. Correlation values significant at 95% are shown in circle.

discussed in Konings and Gentine (2017). For A3, the impact of satellite overpass time on the deviation of predawn condition would not be possible to quantify without field measurements or satellite data over a complete diel cycle, but it can be expected that the timing of AMSR-E observations may lead to potential overestimation (i.e., anisohydric bias) due to the incomplete rehydration at the time of the nighttime (1:30 a.m.) satellite retrieval relative to predawn conditions (also related to A1). For A4, the relative error of the linear relationship on β is small in most cases, except for very dry conditions under which an overestimation of daytime leaf water potential and thus an anisohydric bias could occur (Konings & Gentine, 2017). Nonetheless, uncertainties related to all of these assumptions warrant further investigation.

Second, the definition and quantification of isohydry/anisohydry have been elusive in the literature, and there are alternative metrics to represent the degree of isohydry/anisohydry, ranging from the use of particular water potential values (Meinzer et al., 2009; Skelton et al., 2015) to regression slopes (e.g., Martínez-Vilalta & Garcia-Forner, 2016; Meinzer et al., 2016) or hydroscape area defined by multiple regression lines (Meinzer et al., 2016). The use of different isohydry/anisohydry metrics could result in different rankings of species in their isohydry/anisohydry characterization (Martínez-Vilalta & Garcia-Forner, 2016; Meinzer et al., 2016). Among others, the slope metric is more suitable for satellite-based applications because by definition it is derived from the simple relationship between diurnal changes, which is less dependent on water potential per se, while other metrics are specifically designed based certain features of the water potential measurements (e.g., a threshold or enveloped area). It can thus be estimated even when the quantitative relationship between vegetation water content and water potential is unknown.

Third, the spatially varying vegetated season (similar to growing season) affects the uncertainty of the isohydry/anisohydry estimate, especially at high latitudes. This is because vegetated season determines the time period during which the estimation of β is made and therefore the number of applicable data points. The short vegetated season in the northern high latitudes limits the number of data points available for estimating β (Figure S1), resulting in a larger confidence interval (CI) range in this region relative to other parts of the world (Figure S5). This can be seen in Figure 6a where a longer vegetated season is associated with a reduced CI range in the estimated β for both QuikSCAT σ^0 and AMSR-E VOD. Also, as the vegetated season gets longer, the spatial correlation between σ^0- and VOD-based estimates increases as well, from 0.30 (>1 month) to maximum value of 0.50 (>8 month). Vegetated season length contributes to the larger uncertainty of isohydry/anisohydry estimates over the high latitudes.

Fourth, although both backscatter σ^0 from QuikSCAT and VOD from AMSR-E can reflect vegetation characteristics and are sensitive to vegetation water content (Jones et al., 2011; Steele-Dunne et al., 2012), they are different physical quantities, retrieved at different band frequencies, using different techniques, and with different overpass times, so that the information carried is likely to differ. The different measurement frequencies of σ^0 (Ku-band, 13.4 GHz) and VOD (X-band at 10.7 GHz), though similar, may still affect their penetration

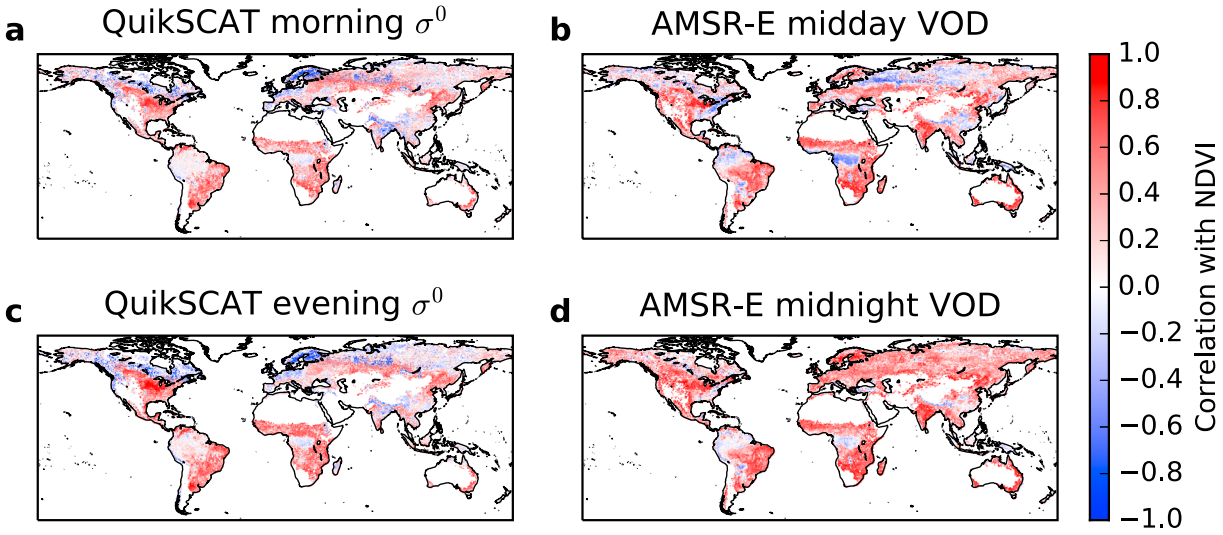

Figure 7. Temporal correlations between time series of AVHRR NDVI and (a) QuikSCAT morning σ^0, (c) evening σ^0, (b) AMSR-E midday VOD, and (d) midnight VOD during the vegetated season of σ^0 for 1999–2009 and VOD for 2002–2011. The correlation is calculated from the half-monthly time series at 0.25° resolution.

capabilities, as well as sensitivities to canopy structure and soil moisture (Guan et al., 2013; Saatchi et al., 2013). While the VOD retrievals isolate the influence of vegetation water content from that of soil moisture, the backscattering coefficients represent the effect of both soil moisture and vegetation (Hardin & Jackson, 2003; Schroeder et al., 2016). The soil moisture component of the Ku-band σ^0 and the residual signal in VOD might still be significant in regions of low vegetation cover or with significant gaps between vegetation patches, such as semiarid grasslands and shrublands, where seasonal variability in vegetation growth and soil moisture is correlated (which is also the rationale for using the EVI threshold to filter out these situations; Frolking et al., 2005). These might be some of the primary reasons to explain the divergence between σ^0- and VOD-based estimates, but further investigation is needed to find and quantify the exact causes. Improved algorithms for retrieving canopy water content from multipolarization backscatter would be helpful to this problem. One potential uncertainty concerning the backscatter signal is the influence of different overpass times (Paget et al., 2016). To test this influence, we utilized another satellite backscatter data set OSCAT (2009–2013) also at Ku-band but having a different overpass time of 12:00 a.m./p.m. The resulting isohydry/anisohydry pattern from OSCAT is more similar to QuikSCAT σ^0-based (spatial correlation, r: 0.39–0.70) than to AMSR-E VOD-based estimates (r: 0.00–0.14) (Table S2). This suggests that overpass time is unlikely to be the main reason for the difference between σ^0- and VOD-based estimates, which is promising for the ability to generate long-term records by combining different low-Earth orbit Ku-band sensors with different overpass times.

Finally, the bias, error, and inconsistency in the microwave satellite data can affect the estimation of isohydry/anisohydry. Both σ^0 and VOD retrievals may show variable sensitivities and biases that are reflected in isohydry/anisohydry patterns. The σ^0 response is sensitive to vegetation canopy structure, which may vary with diurnal and seasonal water stress (Saatchi et al., 2013). The VOD retrieval uncertainty is proportional to canopy biomass and may vary with phenological stage, and diurnal changes in surface temperature (Jones et al., 2011). In addition, both σ^0 and VOD are sensitive to open water, snow cover, and freeze-thaw state variations (Jones et al., 2011; Kimball et al., 2004), particularly at high latitudes. These factors can affect the ability of σ^0 and VOD signals to capture vegetation variability and thereby the estimation of isohydry/anisohydry. Figure 7 shows the temporal correlation between diurnal σ^0/VOD signals and AVHRR NDVI (Normalized difference vegetation index is used to represent vegetation dynamics, obtained from https://ecocast.arc.nasa.gov/data/pub/gimms/3g.v1/) during the vegetated season. It seems that diurnal σ^0 and VOD can capture well vegetation dynamics in most parts of the world, as indicated by their high positive correlation values with NDVI. However, there are discrepancies in many areas, where the correlation is either negative or has a diurnally inconsistent sign, which may suggest problematic vegetation signals in σ^0 and VOD time series. For example, in the eastern U.S., the diurnal AMSR-E VOD time series have negative correlations with NDVI (Figures 7b and 7d; see also (Jones et al., 2011) with EVI), which may reflect an artifact in the VOD retrieval

in eastern deciduous broadleaf forest regions (Jones et al., 2012), whereas in the same region the diurnal QuikSCAT σ^0 still has strong positive correlations with NDVI (see also (Frolking et al., 2006) with EVI). Moreover, there is a large area in the northern high latitudes where the diurnal VOD signals have an inconsistent sign in the correlation with NDVI: negative for midday but positive for midnight (Figures 7b and 7d). These inconsistency issues could be the reason for the much lower β in the VOD estimates (i.e., isohydric bias) in the eastern U.S. and northern high latitudes compared to the σ^0 estimates (Figure 1). Similar issues can be found for σ^0 in Europe (Figures 7a and 7c) where the diurnal σ^0 time series have negative correlations with NDVI, in contrast to the strong positive correlations observed for VOD. This might be the cause for the negative correlation in the direct validation results of the σ^0-based estimate with the upscaled in situ estimates since the GBIF validation data were mainly derived from Europe (Figure 4). The isohydry/anisohydry estimates based on two different VOD data sets show much lower correlation than expected in lower latitude regions (Figure 2), suggesting that different retrieval algorithms (UMT versus LPRM) for the same variable can produce inconsistencies, most likely related to the inversion of both vegetation and soil moisture at once so that the signal can be polluted by soil moisture or because the scattering albedo may not correctly be estimated based on a single measurement (Konings et al., 2016; Konings, Piles, et al., 2017). Such inconsistency issues are not rare in remote sensing; alternative retrievals for variables such as soil moisture (Scipal et al., 2008) and leaf area index (Jiang et al., 2017) sometimes exhibit inconsistent behaviors. All of these uncertainties arising from microwave satellite data can be propagated to the results and thus contribute to regional divergence in σ^0- and VOD-based estimates.

Satellite estimates of isohydry/anisohydry provide useful information about plant water regulation at the ecosystem level as the aggregation of individual species that could exhibit different behaviors (Skelton et al., 2015). It also has direct implications for ecological processes related to plant water use and drought response strategies (Novick et al., 2016). These observations can help us understand the differences in the drought-induced photosynthesis reduction between isohydric and anisohydric ecosystems (Roman et al., 2015), as well as their different sensitivities to environmental factors such as vapor pressure deficit and soil moisture (Konings, Williams, et al., 2017). In addition, there is recent evidence suggesting that besides stomatal behavior, plant isohydry may also be an outcome of other plant traits such as rooting depth and thus should be treated as a whole plant property with respect to plant water regulation status (Martínez-Vilalta & Garcia-Forner, 2016). This suggests that isohydry/anisohydry carries the integrated information of plant water regulation, and the ecosystem level isohydry/anisohydry thus has the promise to provide large-scale constraints on water cycling in ecosystems and upscaling of plant level processes that could greatly improve their prediction and mechanistic representation in ecosystem models.

5. Conclusions

In this study, we used diurnal observations from active (QuikSCAT backscatter) and passive (AMSR-E VOD) microwave remote sensing data to estimate ecosystem isohydry/anisohydry, which is unavailable using traditional physiological methods. The degree of isohydry/anisohydry estimated from QuikSCAT σ^0 and AMSR-E VOD exhibits similar spatial patterns at low and middle latitudes but diverges at high latitudes. The direct validation with in situ measures and indirect validation based on prior knowledge provide additional evidence for a reasonable estimate of isohydry/anisohydry from the two independent satellite data records. However, discrepancies between the σ^0- and VOD-based estimates at high latitude and other regions suggest large uncertainties in the estimates. These uncertainties could arise from a number of methodology-related factors (e.g., isohydry/anisohydry metrics and their assumptions, vegetated season length) and satellite data-related factors (e.g., bias and error in the microwave retrieval) with the latter having been found here to be a primary cause of the discrepancies between the satellite-based isohydry/anisohydry estimates. To improve the robustness of the estimates, several issues related to remote sensing data should be addressed in the future, including a better understanding of the representation of vegetation in microwave remote sensing (active versus passive), reducing uncertainties in the variable retrieval through refined algorithms, and cross validating isohydry/anisohydry estimates from independent microwave remote sensing data. To better validate the ecosystem level satellite estimates, a larger database of in situ measurements covering a broader range of species and locations would reduce the bias in upscaling and alleviate the scale mismatch between the plant and ecosystem level observations. Remote sensing estimation of isohydry/anisohydry is a novel and multidisciplinary topic, integrating other fields such as plant physiology and hydrology. It has great potential

to address ecohydrological problems such as plant water use and drought response (e.g., Konings, Williams, et al., 2017) and also provide large-scale constraints on ecosystem level water regulation that are useful for ecosystem models. These multidisciplinary efforts can deepen our understanding of the large-scale implications of isohydry/anisohydry.

Acknowledgments

Y. L. and K. G. acknowledge the support from the NASA New Investigator Award (NNX16AI56G). P. G. acknowledge the NASA funding (NNX15AB30G). N. G. M. was supported by the Department of Energy, Office of Science, Next Generation Ecosystem Experiment-Tropics and Laboratory Directed Research and Development from Pacific Northwest National Laboratory. Y. L. would like to thank Jin Wu for providing comments on the early version of the manuscript and also Jinyang Du for providing guidance of the VOD data. Y. L. thanks Bin Peng for giving comments on the revised manuscript. We also thank three reviewers and the Editor for their insightful comments that significantly improved the manuscript. This paper was written in Authorea which is a cloud-based collaborative editor for research, and the manuscript is available at www.authorea.com/users/103587/articles/189538. Data of this study are available at figshare (https://figshare.com/projects/Estimating_global_ecosystem_iso_anisohydry_using_active_and_passive_microwave_satellite_data/19492). K. G. and Y. L. designed this study. Y. L. performed the study, and Y. L. and K. G. analyzed the data. W. R. L. A. provided idea of the GBIF analysis. P. G., A. G. K., F. C. M., J. S. K., X. X., W. R. L. A., N. G. M., J. M-V., D. G. L., and S. P. G. provided insights to interpreting the analysis and discussion. Y. L. and K. G. wrote the first draft of the manuscript, and all authors contributed to editing the manuscript.

References

Akıncı, Ş., & Lösel, D. M. (2012). Plant water-stress response mechanisms, Water stress: InTech. https://doi.org/10.5772/29578

Anderegg, W. R. L., Klein, T., Bartlett, M., Sack, L., Pellegrini, A. F. A., Choat, B., & Jansen, S. (2016). Meta-analysis reveals that hydraulic traits explain cross-species patterns of drought-induced tree mortality across the globe. *Proceedings of the National Academy of Sciences of the United States of America*, *113*(18), 5024–5029. https://doi.org/10.1073/pnas.1525678113

Ball, J. T., Woodrow, I. E., & Berry, J. A. (1987). A model predicting stomatal conductance and its contribution to the control of photosynthesis under different environmental conditions. In *Progress in photosynthesis research* (pp. 221–224). Dordrecht, Netherlands: Springer. https://doi.org/10.1007/978-94-017-0519-6_48

Bonan, G. B., Williams, M., Fisher, R. A., & Oleson, K. W. (2014). Modeling stomatal conductance in the Earth system: Linking leaf water-use efficiency and water transport along the soil-plant-atmosphere continuum. *Geoscientific Model Development*, *7*(5), 2193–2222. https://doi.org/10.5194/gmd-7-2193-2014

Domec, J.-C., & Johnson, D. M. (2012). Does homeostasis or disturbance of homeostasis in minimum leaf water potential explain the isohydric versus anisohydric behavior of Vitis vinifera L. cultivars? *Tree Physiology*, *32*(3), 245–248. https://doi.org/10.1093/treephys/tps013

Du, J., Kimball, J. S., Jones, L. A., Kim, Y., Glassy, J., & Watts, J. D. (2017). A global satellite environmental data record derived from AMSR-E and AMSR2 microwave earth observations. *Earth System Science Data*, *9*, 791–808. https://doi.org/10.5194/essd-9-791-2017

Farooq, M., Hussain, M., Wahid, A., & Siddique, M. K. H. (2012). Drought stress in plants: An overview. In *Plant responses to drought stress* (pp. 1–33). Heidelberg: Springer Nature. https://doi.org/10.1007/978-3-642-32653-0_1

Fatichi, S., Pappas, C., & Ivanov, V. Y. (2015). Modeling plant-water interactions: An ecohydrological overview from the cell to the global scale. *Wiley Interdisciplinary Reviews: Water*, *3*(3), 327–368. https://doi.org/10.1002/wat2.1125

Fernandez-Moran, R., Al-Yaari, A., Mialon, A., Mahmoodi, A., Bitar, A. A., … Wigneron, J.-P. (2017). SMOS-IC: An alternative SMOS soil moisture and vegetation optical depth product. *Remote Sensing*, *9*(5), 457. https://doi.org/10.3390/rs9050457

Fisher, R. A., Williams, M., Do, V., Lobo, R., Costa, A. L., & Meir, P. (2006). Evidence from Amazonian forests is consistent with isohydric control of leaf water potential. *Plant, Cell & Environment*, *29*(2), 151–165. https://doi.org/10.1111/j.1365-3040.2005.01407.x

Frolking, S., Fahnestock, M., Milliman, T., McDonald, K., & Kimball, J. (2005). Interannual variability in North American grassland biomass/productivity detected by SeaWinds scatterometer backscatter. *Geophysical Research Letters*, *32*, L21409. https://doi.org/10.1029/2005GL024230

Frolking, S., Milliman, T., McDonald, K., Kimball, J., Zhao, M., & Fahnestock, M. (2006). Evaluation of the SeaWinds scatterometer for regional monitoring of vegetation phenology. *Journal of Geophysical Research*, *111*, D17302. https://doi.org/10.1029/2005JD006588

Garcia-Forner, N., Adams, H. D., Sevanto, S., Collins, A. D., Dickman, L. T., Hudson, P. J., … Mcdowell, N. G. (2015). Responses of two semiarid conifer tree species to reduced precipitation and warming reveal new perspectives for stomatal regulation. *Plant Cell and Environment*, *39*(1), 38–49. https://doi.org/10.1111/pce.12588

Guan, K., Wood, E., & Caylor, K. (2012). Multi-sensor derivation of regional vegetation fractional cover in Africa. *Remote Sensing of Environment*, *124*, 653–665. https://doi.org/10.1016/j.rse.2012.06.005

Guan, K., Wolf, A., Medvigy, D., Caylor, K. K., Pan, M., & Wood, E. F. (2013). Seasonal coupling of canopy structure and function in African tropical forests and its environmental controls. *Ecosphere*, *4*(3), 1–21. https://doi.org/10.1890/es12-00232.1

Guan, K., Wood, E. F., Medvigy, D., Kimball, J., Pan, M., Caylor, K. K., … Jones, M. O. (2014). Terrestrial hydrological controls on land surface phenology of African savannas and woodlands. *Journal of Geophysical Research: Biogeosciences*, *119*, 1652–1669. https://doi.org/10.1002/2013jg002572

Hardin, P. J., & Jackson, M. W. (2003). Investigating seawinds terrestrial backscatter. *Photogrammetric Engineering & Remote Sensing*, *69*(11), 1243–1254. https://doi.org/10.14358/pers.69.11.1243

Jiang, C., Ryu, Y., Fang, H., Myneni, R., Claverie, M., & Zhu, Z. (2017). Inconsistencies of interannual variability and trends in long-term satellite leaf area index products. *Global Change Biology*, *23*, 4133–4146. https://doi.org/10.1111/gcb.13787

Jones, L. A., Kimball, J. S., Podest, E., McDonald, K. C., Chan, S. K., & Njoku, E. G. (2009). A method for deriving land surface moisture, vegetation optical depth, and open water fraction from AMSR-E. In *IEEE International Geoscience and Remote Sensing Symposium, IEEE* (Vol. 2009, pp. III-916–III-919). Cape Town, South Africa. https://doi.org/10.1109/igarss.2009.5417921

Jones, M. O., Jones, L. A., Kimball, J. S., & McDonald, K. C. (2011). Satellite passive microwave remote sensing for monitoring global land surface phenology. *Remote Sensing of Environment*, *115*(4), 1102–1114. https://doi.org/10.1016/j.rse.2010.12.015

Jones, M. O., Kimball, J. S., Jones, L. A., & McDonald, K. C. (2012). Satellite passive microwave detection of North America start of season. *Remote Sensing of Environment*, *123*, 324–333. https://doi.org/10.1016/j.rse.2012.03.025

Kim, Y., Jackson, T., Bindlish, R., Lee, H., & Hong, S. (2012). Radar vegetation index for estimating the vegetation water content of rice and soybean. *IEEE Geoscience and Remote Sensing Letters*, *9*(4), 564–568. https://doi.org/10.1109/lgrs.2011.2174772

Kimball, J., McDonald, K., Frolking, S., & Running, S. (2004). Radar remote sensing of the spring thaw transition across a boreal landscape. *Remote Sensing of Environment*, *89*(2), 163–175. https://doi.org/10.1016/j.rse.2002.06.004

Klein, T. (2014). The variability of stomatal sensitivity to leaf water potential across tree species indicates a continuum between isohydric and anisohydric behaviours. *Functional Ecology*, *28*(6), 1313–1320. https://doi.org/10.1111/1365-2435.12289

Konings, A. G., & Gentine, P. (2017). Global variations in ecosystem-scale isohydricity. *Global Change Biology*, *23*(2), 891–905. https://doi.org/10.1111/gcb.13389

Konings, A. G., Piles, M., Rötzer, K., McColl, K. A., Chan, S. K., & Entekhabi, D. (2016). Vegetation optical depth and scattering albedo retrieval using time series of dual-polarized L-band radiometer observations. *Remote Sensing of Environment*, *172*, 178–189. https://doi.org/10.1016/j.rse.2015.11.009

Konings, A. G., Williams, A. P., & Gentine, P. (2017). Sensitivity of grassland productivity to aridity controlled by stomatal and xylem regulation. *Nature Geoscience*, *10*, 284–288. https://doi.org/10.1038/ngeo2903

Konings, A. G., Yu, Y., Xu, L., Yang, Y., Schimel, D. S., & Saatchi, S. S. (2017). Active microwave observations of diurnal and seasonal variations of canopy water content across the humid African tropical forests. *Geophysical Research Letters*, *44*, 2290–2299. https://doi.org/10.1002/2016GL072388

Konings, A. G., Piles, M., Das, N., & Entekhabi, D. (2017). L-band vegetation optical depth and effective scattering albedo estimation from SMAP. *Remote Sensing of Environment*, *198*, 460–470. https://doi.org/10.1016/j.rse.2017.06.037

Landsberg, J., & Waring, R. (2016). Water relations in tree physiology: Where to from here? *Tree Physiology*, *37*, 18–32. https://doi.org/10.1093/treephys/tpw102

Long, D. G., & Hicks, B. R. (2010). Standard BYU QuikSCAT/SeaWinds land/ice image products. Provo, UT: Brigham Young University. Retrieved from www.scp.byu.edu/docs/pdf/QscatReport6.pdf

Martínez-Vilalta, J., & Garcia-Forner, N. (2016). Water potential regulation, stomatal behaviour and hydraulic transport under drought: Deconstructing the iso/anisohydric concept. *Plant, Cell & Environment*, *40*, 962–976. https://doi.org/10.1111/pce.12846

Martínez-Vilalta, J., Poyatos, R., Aguadé, D., Retana, J., & Mencuccini, M. (2014). A new look at water transport regulation in plants. *New Phytologist*, *204*(1), 105–115. https://doi.org/10.1111/nph.12912

Matheny, A. M., Fiorella, R. P., Bohrer, G., Poulsen, C. J., Morin, T. H., Wunderlich, A., … Curtis, P. S. (2016). Contrasting strategies of hydraulic control in two codominant temperate tree species. *Ecohydrology*, *10*, E1815. https://doi.org/10.1002/eco.1815

McDowell, N., Pockman, W. T., Allen, C. D., Breshears, D. D., Cobb, N., Kolb, T., … Yepez, E. A. (2008). Mechanisms of plant survival and mortality during drought: Why do some plants survive while others succumb to drought? *New Phytologist*, *178*(4), 719–739. https://doi.org/10.1111/j.1469-8137.2008.02436.x

McDowell, N. G., Fisher, R. A., Xu, C., Domec, J. C., Hölttä, T., Mackay, D. S., … Pockman, W. T. (2013). Evaluating theories of drought-induced vegetation mortality using a multimodel-experiment framework. *New Phytologist*, *200*(2), 304–321. https://doi.org/10.1111/nph.12465

Meesters, A., DeJeu, R., & Owe, M. (2005). Analytical derivation of the vegetation optical depth from the microwave polarization difference index. *IEEE Geoscience and Remote Sensing Letters*, *2*(2), 121–123. https://doi.org/10.1109/lgrs.2005.843983

Meinzer, F. C., Johnson, D. M., Lachenbruch, B., McCulloh, K. A., & Woodruff, D. R. (2009). Xylem hydraulic safety margins in woody plants: Coordination of stomatal control of xylem tension with hydraulic capacitance. *Functional Ecology*, *23*(5), 922–930. https://doi.org/10.1111/j.1365-2435.2009.01577.x

Meinzer, F. C., Woodruff, D. R., Marias, D. E., Smith, D. D., McCulloh, K. A., Howard, A. R., & Magedman, A. L. (2016). Mapping 'hydroscapes' along the iso- to anisohydric continuum of stomatal regulation of plant water status. *Ecology Letters*, *19*(11), 1343–1352. https://doi.org/10.1111/ele.12670

Novick, K. A., Miniat, C. F., & Vose, J. M. (2016). Drought limitations to leaf-level gas exchange: Results from a model linking stomatal optimization and cohesion-tension theory. *Plant Cell & Environment*, *39*(3), 583–596. https://doi.org/10.1111/pce.12657

Owe, M., de Jeu, R., & Holmes, T. (2008). Multisensor historical climatology of satellite-derived global land surface moisture. *Journal of Geophysical Research*, *113*, F01002. https://doi.org/10.1029/2007JF000769

Paget, A. C., Long, D. G., & Madsen, N. M. (2016). Rapidscat diurnal cycles over land. *IEEE Transactions on Geoscience and Remote Sensing*, *54*(6), 3336–3344. https://doi.org/10.1109/tgrs.2016.2515022

Pekel, J.-F., Cottam, A., Gorelick, N., & Belward, A. S. (2016). High-resolution mapping of global surface water and its long-term changes. *Nature*, *540*(7633), 418–422. https://doi.org/10.1038/nature20584

Podest, E., McDonald, K. C., & Kimball, J. S. (2014). Multisensor microwave sensitivity to freeze/thaw dynamics across a complex boreal landscape. *IEEE Transactions on Geoscience and Remote Sensing*, *52*(11), 6818–6828. https://doi.org/10.1109/tgrs.2014.2303635

Roman, D. T., Novick, K. A., Brzostek, E. R., Dragoni, D., Rahman, F., & Phillips, R. P. (2015). The role of isohydric and anisohydric species in determining ecosystem-scale response to severe drought. *Oecologia*, *179*(3), 641–654. https://doi.org/10.1007/s00442-015-3380-9

Saatchi, S., Asefi-Najafabady, S., Malhi, Y., Aragao, L. E. O. C., Anderson, L. O., Myneni, R. B., & Nemani, R. (2013). Persistent effects of a severe drought on Amazonian forest canopy. *Proceedings of the National Academy of Sciences of the United States of America*, *110*(2), 565–570. https://doi.org/10.1073/pnas.1204651110

Schroeder, R., McDonald, K. C., Azarderakhsh, M., & Zimmermann, R. (2016). ASCAT MetOp-A diurnal backscatter observations of recent vegetation drought patterns over the contiguous U.S.: An assessment of spatial extent and relationship with precipitation and crop yield. *Remote Sensing of Environment*, *177*, 153–159. https://doi.org/10.1016/j.rse.2016.01.008

Schultz, H. R. (2003). Differences in hydraulic architecture account for near-isohydric and anisohydric behaviour of two field-grown Vitis vinifera L. cultivars during drought. *Plant Cell & Environment*, *26*(8), 1393–1405. https://doi.org/10.1046/j.1365-3040.2003.01064.x

Scipal, K., Holmes, T., de Jeu, R., Naeimi, V., & Wagner, W. (2008). A possible solution for the problem of estimating the error structure of global soil moisture data sets. *Geophysical Research Letters*, *35*, L24403. https://doi.org/10.1029/2008GL035599

Skelton, R. P., West, A. G., & Dawson, T. E. (2015). Predicting plant vulnerability to drought in biodiverse regions using functional traits. *Proceedings of the National Academy of Sciences of the United States of America*, *112*(18), 5744–5749. https://doi.org/10.1073/pnas.1503376112

Sperry, J. S., Wang, Y., Wolfe, B. T., Mackay, D. S., Anderegg, W. R. L., McDowell, N. G., & Pockman, W. T. (2016). Pragmatic hydraulic theory predicts stomatal responses to climatic water deficits. *New Phytologist*, *212*(3), 577–589. https://doi.org/10.1111/nph.14059

Steele-Dunne, S. C., Friesen, J., & van de Giesen, N. (2012). Using diurnal variation in backscatter to detect vegetation water stress. *IEEE Transactions on Geoscience and Remote Sensing*, *50*(7), 2618–2629. https://doi.org/10.1109/tgrs.2012.2194156

Steele-Dunne, S. C., McNairn, H., Monsivais-Huertero, A., Judge, J., Liu, P.-W., & Papathanassiou, K. (2017). Radar remote sensing of agricultural canopies: A review. *IEEE Journal of Selected Topics in Applied Earth Observations and Remote Sensing*, *10*(5), 2249–2273.

Tardieu, F., & Simonneau, T. (1998). Variability among species of stomatal control under fluctuating soil water status and evaporative demand: Modelling isohydric and anisohydric behaviours. *Journal of Experimental Botany*, *49*(90001), 419–432. https://doi.org/10.1093/jexbot/49.suppl_1.419

Ulaby, F., & Long, D. (2014). *Microwave radar and radiometric remote sensing*. Ann Arbor, MI: University of Michigan Press. https://doi.org/10.3998/0472119356

van Emmerik, T., Steele-Dunne, S. C., Judge, J., & van de Giesen, N. (2015). Impact of diurnal variation in vegetation water content on radar backscatter from maize during water stress. *IEEE Transactions on Geoscience and Remote Sensing*, *53*(7), 3855–3869. https://doi.org/10.1109/tgrs.2014.2386142

van Emmerik, T., Steele-Dunne, S. C., Judge, J., & Giesen, N. V. D. (2017). Dielectric response of corn leaves to water stress. *IEEE Geoscience and Remote Sensing Letters*, *14*(1), 8–12. https://doi.org/10.1109/lgrs.2016.2606662

van Emmerik, T., Steele-Dunne, S., Paget, A., Oliveira, R. S., Bittencourt, P. R. L., Barros, F. deV., & van de Giesen, N. (2017). Water stress detection in the Amazon using radar. *Geophysical Research Letters*, *44*, 6841–6849. https://doi.org/10.1002/2017gl073747

Waring, R. H., Way, J., Hunt, E. R., Morrissey, L., Ranson, K. J., Weishampel, J. F., … Franklin, S. E. (1995). Imaging radar for ecosystem studies. *BioScience*, *45*(10), 715–723. https://doi.org/10.2307/1312677

Wong, S. C., Cowan, I. R., & Farquhar, G. D. (1979). Stomatal conductance correlates with photosynthetic capacity. *Nature*, *282*(5737), 424–426. https://doi.org/10.1038/282424a0

Xu, C., McDowell, N. G., Sevanto, S., & Fisher, R. A. (2013). Our limited ability to predict vegetation dynamics under water stress. *New Phytologist*, *200*(2), 298–300. https://doi.org/10.1111/nph.12450

Xu, X., Medvigy, D., Powers, J. S., Becknell, J. M., & Guan, K. (2016). Diversity in plant hydraulic traits explains seasonal and inter-annual variations of vegetation dynamics in seasonally dry tropical forests. *New Phytologist*, *212*(1), 80–95. https://doi.org/10.1111/nph.14009